AIMS Geosciences

AIMS Geosciences, 11(4): 993–1006.
DOI: 10.3934/geosci.2025043
Received: 23 July 2025
Revised: 10 October 2025
Accepted: 28 October 2025
Published: 28 November 2025

https://www.aimspress.com/journal/geosciences

Research article

Regional surface temperature changes in China caused by reduced air pollution and halogenated greenhouse gases

Kaiyun Zhang[1,2], Kejian Ding[2,*] and Qing-Bin Lu[1,*]

[1] Department of Physics and Astronomy, University of Waterloo, 200 University Avenue West, Waterloo, Ontario N2L 3G1, Canada
[2] School of Physical Science and engineering, Beijing Jiaotong University, No.3 Shangyuancun, Haidian District, Beijing 100044, P. R. China

* **Correspondence:** Email: dkjian@bjtu.edu.cn; qblu@uwaterloo.ca; Tel: +1-519-888-4567.

Abstract: China's vast territory across a large latitude makes it an ideal country to investigate the mechanisms causing regional climate changes. Here, we showed that the temporal patterns in regional surface temperature are very different between low- and high latitude regions and between lightly and severely polluted regions, and that a reversal in surface temperature occurs earlier at higher-latitude regions. The latter is affected by recent drastic reductions in air pollution, which give rise to positive net radiative forcings that are the primary cause for China's regional temperature rises in the last decade. These regional climate patterns are in good agreement with both the cosmic-ray driven electron-induced reaction (CRE) theory of ozone depletion and the physics model of warming caused by halogen-containing greenhouse gases (halo-GHGs, mainly chlorofluorocarbons (CFCs)). Using the IPCC-given globally averaged radiative forcings of aerosols and ozone, our calculated results by the CFC-warming physics model showed good agreement with the observed regional surface temperature changes since 1990, giving correlation coefficients of 0.70–0.96. In lightly polluted regions, such as northeast and northwest China (Heilongjiang, Xinjiang and Inner Mongolia), Hainan and Guangdong, our calculations reproduced close observations, while underestimating temperatures in highly polluted regions such as Beijing (Hebei), Fujian, and Jiangsu. This discrepancy is explained by larger reductions in post-2013 air pollution, causing greater positive radiative forcings. Our results revealed the mechanisms for regional and global climate change.

Keywords: air pollution; climate change; halogenated greenhouse gases (halo-GHGs); regional climate change patterns; quantitative analysis; the CFC-warming physics model; the cosmic-ray driven electron-induced reaction (CRE) theory of ozone depletion.

1. Introduction

In the early 2000s, China suffered from severe air pollution due to its rapid economic development and industrialization [1]. With the implementation of active clean air policies, China has substantially reduced air pollution since the early 2010s [2,3]. A study of China's anthropogenic emission trends from 2010 to 2017 by Zheng et al. [2] showed the following changes: +16 % for CO_2, −62 % for SO_2, −17 % for NO_x, −38% for PM10, −35 % for PM2.5, −27 % for black carbon, and −35 % for organic carbon. These reductions were mainly due to emission control measures on power plants and industries, and the majorities of these reductions occurred after 2013. The marked acceleration of the reduction rates of China's anthropogenic emissions demonstrates the effectiveness of China's Clean Air Action implemented since 2013. Air pollutants, such as PM2.5, surface ozone, and their precursors, have lifetimes long enough in the troposphere to be transported to other regions. Thus, China's emission changes affect air quality not only in China but also in other regions. For the same period 2010–2017, Zhang et al. [3] performed another independent study, using a global chemistry transport model to simulate the impact of Chinese emission changes on both domestic and foreign air quality. Their simulated results showed that the population-weighted annual PM2.5 concentration in China peaked in 2011, and that the emission sharply decreased after 2013, consistent with the observations by Zheng et al. [2]. Zhang et al. [3] also showed that the population-weighted, annually averaged ozone concentration peaked in 2014 and decreased relatively slowly by 2017.

Spatially, Zhang et al.[3] showed that significant PM2.5 changes (increased before 2013 and decreased thereafter) mainly occurred in eastern China and that there were increasing ozone trends mostly in the Beijing-Tianjin-Hebei and Yangtze River Delta regions and slightly decreasing trends in the south. They also showed that there has been very little air pollution in northeast and northwest China (particularly in Heilongjiang, Inner Mongolia, and Xinjiang). In downwind regions to China, countries such as South Korea, Japan, and the United States generally experienced O_3 reductions following 2013 due to the decreased export of ozone and its precursors from China. In both studies [2,3], the observed and/or simulated data consistently demonstrated that air pollutions in China have sharply reduced over the past decade, which have also contributed to the substantial improvement of air quality on a global scale (in particularly other parts of East Asia) [3].

In 2020, the Chinese government announced its aims for the country to reach its peak CO_2 emissions before 2030 and achieve carbon neutrality by 2060 in line with the Paris Agreement. However, CO_2-based climate models estimate that such a pathway still leads to ~3 °C temperature rise. The IPCC AR6 [4] assessed the spatiotemporal evolutions of tropospheric aerosols and ozone. Sulfate measured from ice cores increased by factors of 3–8 in various regions, including the Arctic, Russia, and continental Europe from the end of the 19th century. In all regions studied, the sulfate concentrations have declined by a factor of about 2 following their peak (~1970 in Europe and Russia, and 1950 in the Arctic). Similar increases in black carbon were observed over Europe, Russia,

Greenland (primarily originating from emissions from North America), and in the Arctic in the 20th century. The IPCC AR6 [4] also assessed large-scale trends in aerosol optical depths (AODs) by satellite- and ground-based measurements over 2000–2019. The AOD data showed significant declining trends over Europe, Russia, and North America; the tendency over East Asia reversed from positive (2000–2010) to negative (since 2010), which is generally consistent with the above-mentioned observations of air quality in China [2,3]; and there have been positive trends over Southern Asia and East Africa. These trends have led to a globally decreasing trend of aerosol abundance and a corresponding positive trend in aerosol effective radiative forcings (ERF). The IPCC AR6 also estimated tropospheric ozone trends, which has significantly increased in most regions of the globe except the Antarctic since the mid-20th century.

Simulated results by climate models in the IPCC AR6 [4] showed that although the short-term ERFs of aerosols and ozone associated with air pollution on the global scale essentially canceled out during the period 1970–2010, they have led to a positive net forcing of 0.4–0.5 W/m^2 from around 2010 up to the present [5]. This gives rise to complexities in surface temperature change in the regions such as Northern Hemisphere (NH) mid-latitudes that are experiencing drastic changes in level of air pollution, adding to the greenhouse effect of well-mixed greenhouse gases (WM-GHGs). For example, Yang et al. [6] investigated the role of remote and local aerosols on the regional climate in the Western United States and early 2020 (during the COVID-19 pandemic) and found that the reduction in aerosols resulted in higher temperatures (up to ∼0.5 °C) and generally lower snow amounts over this region. The study improved our understanding of the effect of local and remote aerosols on precipitation and temperature across the western United States. Another example is a study of regional mean changes in surface air temperature due to changes in GHGs, aerosol emissions, and tropospheric O_3 levels by Wang et al. [7], who showed that in 2050 under a carbon neutrality pathway, warming caused by aerosol reductions would dominate climate change over the (sub)regions with surface air temperature increases by 0.5–1.4 °C, which are much higher than the GHG-caused surface temperature increases of ≤0.2 °C, and the tropospheric O_3 caused surface temperature decreases of ≤0.2 °C. Despite their well-known large uncertainties in magnitude, simulated ERFs of aerosols and ozone given in the AR6 [4] should have been better constrained by increasing satellite- and ground-based observations of aerosol loadings and ozone since the 1990s.

As reviewed in [5], there are major differences between CO_2-based climate models (i.e., general circulation models (GCMs)) and the chlorofluorocarbon (CFC)-warming physics model. GCMs are "*quasi-realistic*", which not only include unresolved terms represented in equations with tunable parameters but also have major limitations such as the requirement of tuning the models to match the observed temperatures and the structural error and uncertainty across models [8]. In contrast, the CFC-warming model, which was developed on the basis of an empirical linear model developed by Lean and Rind [9], is a conceptual physics model that includes no tunable parameters and can perform analytical calculations of variations in global mean surface temperature (GMST) caused by halogen-containing GHGs (halo-GHGs), ozone, aerosols, and solar variability [5,10–12]. This CFC-warming physics model has predicted a long-term turnover in GMST, corresponding to the changing trend of atmospheric halo-GHGs [5,10–12]. Furthermore, according to the cosmic-ray (CR) driven electron-induced reaction (CRE) theory of global ozone depletion [10,13–17], the destruction by the CRE reaction of ozone-depleting substances (ODSs), which are also major halo-GHGs, is increasingly effective with increasing latitudes due to increasing CR fluxes. As a direct consequence, the CFC-

warming and CRE models have predicted that the reversals in global climate change and ozone depletion due to anthropogenic emissions of ODSs (halo-GHGs) will occur earlier at higher latitudes, especially the polar regions where the levels of halo-GHGs/ODSs (mainly CFCs) decrease first; such reversals will lag by about 10 years in the tropics or low latitudes [5,10,11,15]. The predicted reversal in surface warming (i.e., a cooling trend), however, is complicated by short-term ERFs of aerosols and ozone associated with air pollution [12]. The ODS-related O_3 recovery at high latitudes since the mid-1990s has been observed by Lu [10,15,17] and others [18,19]. Moreover, Philipona et al. [20] analyzed upper-air radiosonde temperature profiles from 1976 to 2015, showing that after decades of cooling, the lower stratosphere at altitudes between 15 and 30 km and over most continents has now been warming since the turn of the century. This reversal in lower-stratospheric temperature was confirmed in a study by Lu [11], who used the EUMETSAT's ROM SAF satellite datasets of the troposphere-stratosphere temperature climatology. Lu [11,12] discovered that such a temperature reversal has also occurred in the upper stratosphere at altitudes above 30 km over the past decade, especially at high latitudes. Consistently, a reversal from warming to cooling on the surface has been observed in the Antarctic since 2002 [5] and in the Arctic since 2016 when the Arctic amplification effect associated with sea-ice melting on surface temperature stopped [12]. Moreover, the CFC-warming physics model reproduces closely the observed GMSTs from 2000 to 2024, including almost no warming during 2000–2012 and the significant warming by 0.2–0.3 °C during 2013–2023, of which 0.23–0.27 °C was calculated to arise from the net radiative forcing of aerosols and ozone due to improved air quality [12]. Thus, the CFC-warming and CRE mechanisms are in good agreement with the observations of patterns in global lower-stratospheric temperature (ozone) and GMST reported in these studies [5,11,12,16,17,20]. Consistent with our finding [12], Goessling et al. [21], using satellite and reanalysis data, identified a record-low planetary albedo as the primary factor leading to the GMST in 2023 of about 0.2 K higher than that caused by known drivers, including anthropogenic warming and the El Niño onset. The albedo reduction is apparently largely due to a pronounced decline of low-level clouds over the northern mid-latitude and tropics, in continuation of a multiannual trend. They found that the increased absorption of shortwave radiation since December 2020, due to reduced albedo, can explain 0.22 ± 0.04 K of the 2023 temperature rise. For a comprehensive review of the CFC-warming physics model of global climate change and the CRE mechanism of global ozone depletion, which have both been developed into complete quantitative theories with no adjustable parameters, the readers are referred to the forthcoming monograph [22].

Moreover, since climate is a complex system, accurate climate predictions need understanding of not only external drivers but also internal variability (atmospheric dynamics) [4]. Apart from non-stationarities (e.g., trends and cycles), there may exist persistent correlations of the temporal fluctuations in GMST anomalies. In other words, correlations or other intrinsic variabilities may be hidden in the time-series GMSTs. For example, Varotsos and co-workers [23], using the detrended fluctuation analysis (DFA) method, revealed that there existed persistent long-range power-law correlations, for all time lags between 4 months and 39 years, in the detrended time-series GMST anomalies during the period January 1850–August 2008, stemming from the time evolution of the GMST anomalies. Such studies using the DFA method could enhance the reliability of climate dynamics modeling and improve the accuracy of global climate models to predict future climate changes. Nevertheless, we focus on the trend analysis of surface temperatures in various regions in China and neglects the DFA. For a more accurate and comprehensive analysis, the DFA method should be applied.

China is the third-largest country by total land area with an area of ~9.6 million km^2, whose territory is vast, lying between latitudes 18° and 54° N, and longitudes 73° and 135° E. China's landscapes vary significantly across its territory, and the climate is highly inhomogeneous. Its diverse landscapes and highly inhomogeneous provincial-level population densities and industrial developments lead to pronounced differences in air pollution levels across the country, as observed in studies [2,3]. These features make China a very interesting country to investigate the mechanisms underlying regional climate changes. To study the regional surface temperature changes in China, we divide its geographical territory into four latitude bands 20°–30° N, 30°–40° N, 40°–50° N, and 50°–60°N in the longitude range 75°–135° E, as shown in Figure 1. This study will represent the first application of the CFC-warming physics model and the CRE mechanism to understanding regional climate changes in a country. We aim to unravel the major mechanism underlying the large differences in surface temperature trends in regions across China in the past two decades.

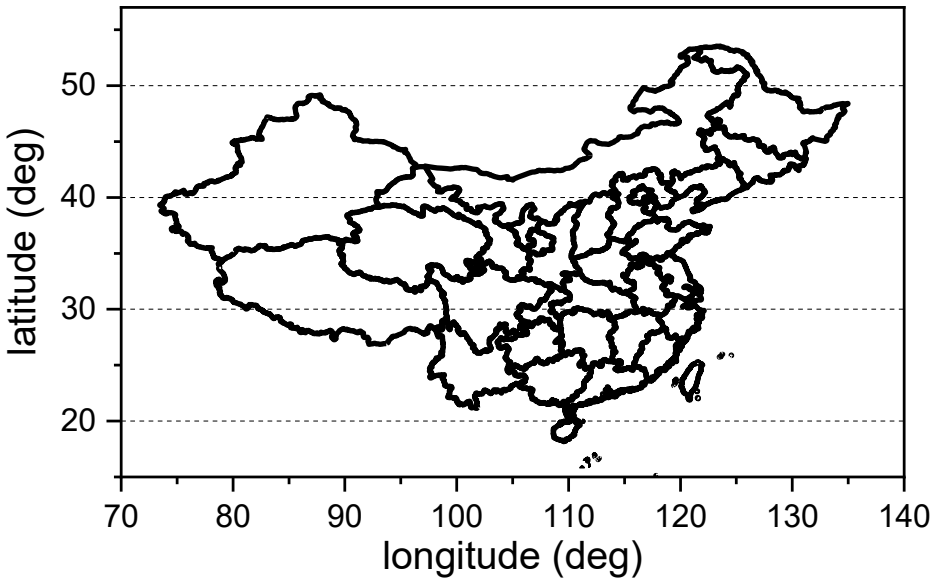

Figure 1. The map of China, showing its geographical territory divided into four latitude bands 20°–30° N, 30°–40° N, 40°–50° N, and 50°–60°N in the longitude range 75°–135° E.

2. Materials (Data) and methods

Trends of aerosols (AOD) at measurement stations in China are derived from the ground-based solar attenuation AERONET network [24]. Surface temperature data are obtained from the NOAA Global Surface Temperature Dataset (NOAAGlobalTemp), Version 6.0.0 [25,26]. Note that the regional surface temperatures in observed data are affected by the natural climate drivers such as El Niño southern oscillation (ENSO) and volcanic effects. ENSO has been the largest source of year-to-year variability, exerting its global impacts and affecting extreme weather events [27,28]. The data of total solar irradiance (TSI), concentrations of halo-GHGs, effective radiative forcings of ozone and aerosols were obtained from the IPCC AR6 [4].

To give quantitative estimates of regional surface temperature changes in China since 1990, we use the CFC-warming physics model with details given previously [5,10]. This CFC model was

modified to include the (effective) radiative forcings (RFs) (ERFs) of aerosols and ozone, in addition to halo-GHGs and solar variability, giving the surface temperature change by [12]

$$\Delta T_s = \lambda_c^{halo} \times (RF^{halo} + RF^{O3}) + \lambda_c^s \times (RF^{solar} + RF^{aerosol}), \quad (1)$$

where $\lambda_c^s = 0.46\ K/(Wm^{-2})$ determined by an observational approach and $\lambda_c^{halo} = 1.77\ K/(Wm^{-2})$ determined from the energy spectrum of the Earth's blackbody radiation given by Planck's formula and the measured atmospheric transmittance spectrum [10]. A slightly larger $\lambda_c^s = 0.63\ K/(Wm^{-2})$ was equivalently derived by Douglass and Clader [29], who used a larger GMST variation amplitude (±0.15 °C) in 11-year solar cycles. The latter has been determined to be ±0.11 °C in more recent and reliable measurements [10]. Thus, we use $\lambda_c^s = 0.46\ K/(Wm^{-2})$ in this study, consistent with the previous studies [5,10,11]. Notably, there are no tunable parameters in this conceptual physics model, which is in marked contrast to GCMs [8] and the Lean-Rind empirical linear model [9]. Time-series RFs of halo-GHGs and solar variability are analytically calculated from the surface (lower troposphere)-measured concentrations of halo-GHGs and the TSIs, respectively [5,10], where time lags Δt = 10, 5, and 0 yr are applied to RFs (ERFs) of halo-GHGs at lower-latitudes (20°–30° N and 30°–40° N), intermediate latitudes 40°–50° N, and higher-latitudes 50°–60°N respectively. These lags are inferred from the latitude-dependent decomposition efficiencies of halogenated gases through the CRE mechanism and the observed recoveries of the ozone layers over the regions [5,10,11,15,17,22]. It is difficult to make quantitative estimates of regional RFs of aerosols and ozone in various regions in China. To obtain a quantitative understanding of regional climate changes in China, however, we might as well use the globally mean ERFs of aerosols and ozone given in the IPCC AR6 [4], which should have a reasonably good certainty since 1990, and then consider the differences in level of air pollution between the regions in China and the entire globe. Given these RFs (ERFs), our theoretical calculations by Eq. 1 give time-series surface temperature changes at various regions in China.

3. Results and discussion

3.1. Air quality and aerosol observations

Figure 2 shows the measured surface-level concentrations of major pollutants SO_2, NO_x, and $PM_{2.5}$ from national air quality monitoring stations in China for the period of 2013–2017, which were validated by satellite-derived retrievals from the DOMINO V2 product and the Ozone Monitoring Instrument (OMI) V3 product by Zheng et al. [2]. Time-series data of AODs in various locations in China obtained from the AERONET network [24] are shown in Figure 3. These AOD results show that aerosol levels in most regions of China have indeed been decreasing significantly since around 2013, consistent with the measured surface concentration changes of pollutants shown in Figure 2.

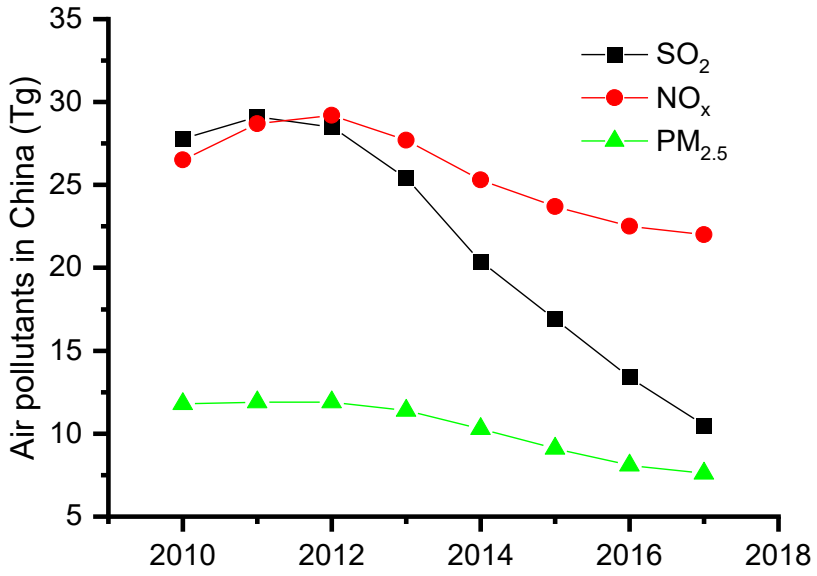

Figure 2. Anthropogenic emissions of major air pollutants in China from 2010 to 2017, plotted with the tabulated data obtained from Zheng et al. [2].

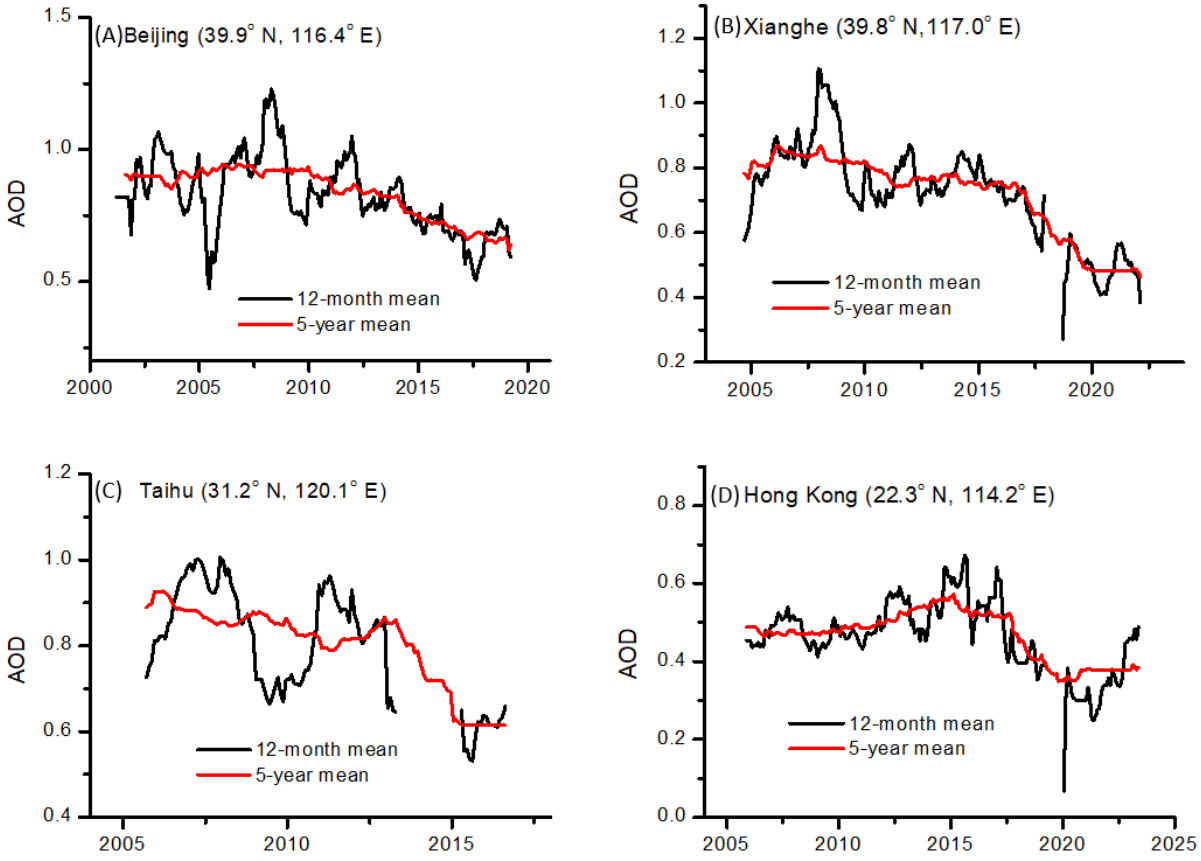

Figure 3. Time-series AODs at representative measurement stations in China, obtained from the AERONET network.

3.2. Observed and modeled regional climate patterns

Regional surface temperature changes in the period 1950–2024 in the four latitude bands 20°–30° N, 30°–40° N, 40°–50° N, and 50°–60°N across China are shown in Figure 4, while surface temperature changes at the representative provinces/territories/cities are shown in Figure 5. Our theoretically calculated surface temperatures since 1990 are also shown in Figures 4 and 5 with given linear correlation coefficients (Rs) and root mean square errors (RMSEs) between observed and CFC theoretical surface temperatures, while the corresponding residuals of observed surface temperatures after the subtraction of the CFC theoretical values are shown in Figure 6A and B. The temperatures are with respect to their means in 1995–2005. The major findings are the following: First, the observed data show very interesting results: The temperatures at the high-latitude band 50–60° N (Figure 4A) and in the northeast Province Heilongjiang (Figure 5C) reached a plateau in the early 1990s with a nearly zero lag ($\Delta t = 0$ yr) to the ERF peak of surface-measured halo-GHGs, while the temperatures reached a plateau with a lag of about 5 years ($\Delta t = 5$ yr) at the intermediate latitude band 40–50° N (Figure 4B) or the northwest China (Inner Mongolia and Xinjiang) and Beijing (Hebei) (Figure 5A, B, and F) and with a lag of ~10 years ($\Delta t = 10$ yr) at lower latitudes below 40° N (Figure 4C-D) or east and southeast China (Sichuan, Jiangsu, Hainan, Guangdong, Fujian) (Figure 5D-E and G-I). These temporal patterns are consistent with what are expected from the CRE mechanism of halo-GHGs (ODSs) and with the observed difference between the recoveries of the ozone layers at high and low latitudes [10,18,19,22,30,31], indicating that ozone depletion and global warming originate from halogenated gases that are decomposed in the atmosphere through the CRE mechanism [5,11–14,16,17,22]. Note that in Figure 4, the correlation coefficients Rs = 0.77 and 0.81 for higher-latitude regions 50°–60°N and 40°–50° N, respectively, are smaller than that (R = 0.94) for lower-latitude regions 30°–40°N and 20°–30° N. This appears surprizing, but it is caused by the fact that the (observed) surface temperatures at the higher-latitude regions have exhibited much weaker or almost no trends over the last 2–3 decades, most obvious for the most northeast province Heilongjiang (see Figure 5C and discussion below). Figure 6A also shows that the residual in the last decade for the latitude band 50–60° N, which is near the Arctic, is somewhat larger than lower-latitude bands. However, this is not surprizing as surface warming at this higher latitude region is much greater (Figure 4A), which is most likely due to the influence by the well-known Arctic Amplification.

Second, most remarkably, our theoretical calculations show that in northeast, northwest, and south China, namely the provinces/territories of Heilongjiang, Inner Mongolia, Xinjiang, Hainan, and Guangdong, where air pollution has always been insignificant or moderate [3], the calculated surface temperature changes using the globally averaged ERFs of aerosols and ozone exhibit excellent agreement with the observed data with minimal discrepancies (residuals) (Figure 5A, B, C, G and H; Figure 6B). Again, the obtained lowest correlation coefficient R = 0.70 for Heilongjiang (Figure 5C) does not indicate poor agreement between observed and CFC modeled data. Instead, this lowest R value is caused by the fact that the (observed) surface temperature at this most northeastern province in China has become rather stable (almost no trend) since the early 1990s, where the residual (discrepancy) between the observed temperatures and CFC theoretical values is the smallest and within the noisy level (Figure 6B). These results indicate that the CFC-warming physics model has well captured the major features of regional surface temperature changes.

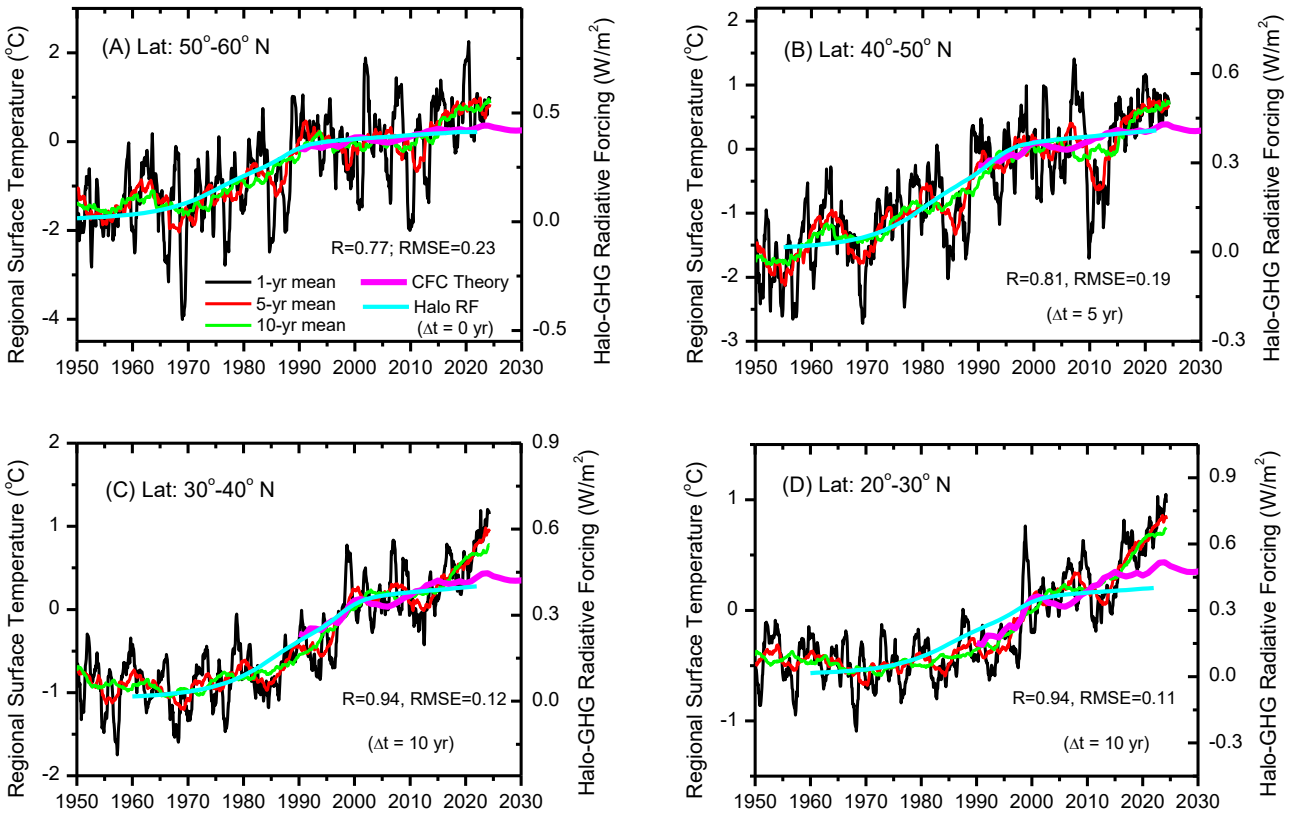

Figure 4. Time-series observed and calculated regional surface temperature changes in the four latitude bands 20°–30° N, 30°–40° N, 40°–50° N, and 50°–60°N across China, where the observed temperature data are processed by 1-, 5- and 10-year smoothing, and time-series global mean (effective) radiative forcing (RF/ERF) of halo-GHGs is also shown with the lag (Δt) indicated. The temperatures are relative to their means in 1995–2005. In each of A to D, statistical analysis gives a linear correlation coefficient (R) and root mean square error (RMSE) for the observed 10-year mean GMSTs and no-parameter CFC model.

Third, we note that our calculated results underestimate the observed temperatures over the past decade in east and southeast China, the Beijing–Tianjin–Hebei, and Yangtze River Delta regions, mostly at the latitude bands 30°–40° N and 20°–30° N. As shown in Figure 5D, E, F, and I and Figure 6B, the provinces/regions Beijing (Hebei), Fujian, Jiangsu, and Sichuan exhibit high R values in the range 0.90–0.96 but have the largest discrepancies (positive residuals) up to ~0.5 °C over the last decade. As shown by Zhang et al. [3], these regions once had most severe air pollution prior to 2010, which was much severer than the global average and was largely reduced in the past decade. Although the reliable net positive regional (local) ERFs of aerosol and ozone levels in these regions are not available, they are expected to be significantly larger than the global mean values. Thus, our calculated results of regional surface temperatures are very reasonably expected: Since we use the globally mean net positive ERFs of aerosols and ozone arising from the global mean air pollution reduction, our calculated temperatures in these regions that were once highly polluted are somewhat lower than the observed ones. These results are also in good agreement with the conclusion reached in [12], where global mean surface warming in the past two decades (particularly in the period 2013–2023) was

mainly caused by the short-term radiative forcings of aerosols and ozone associated with global air pollution reductions.

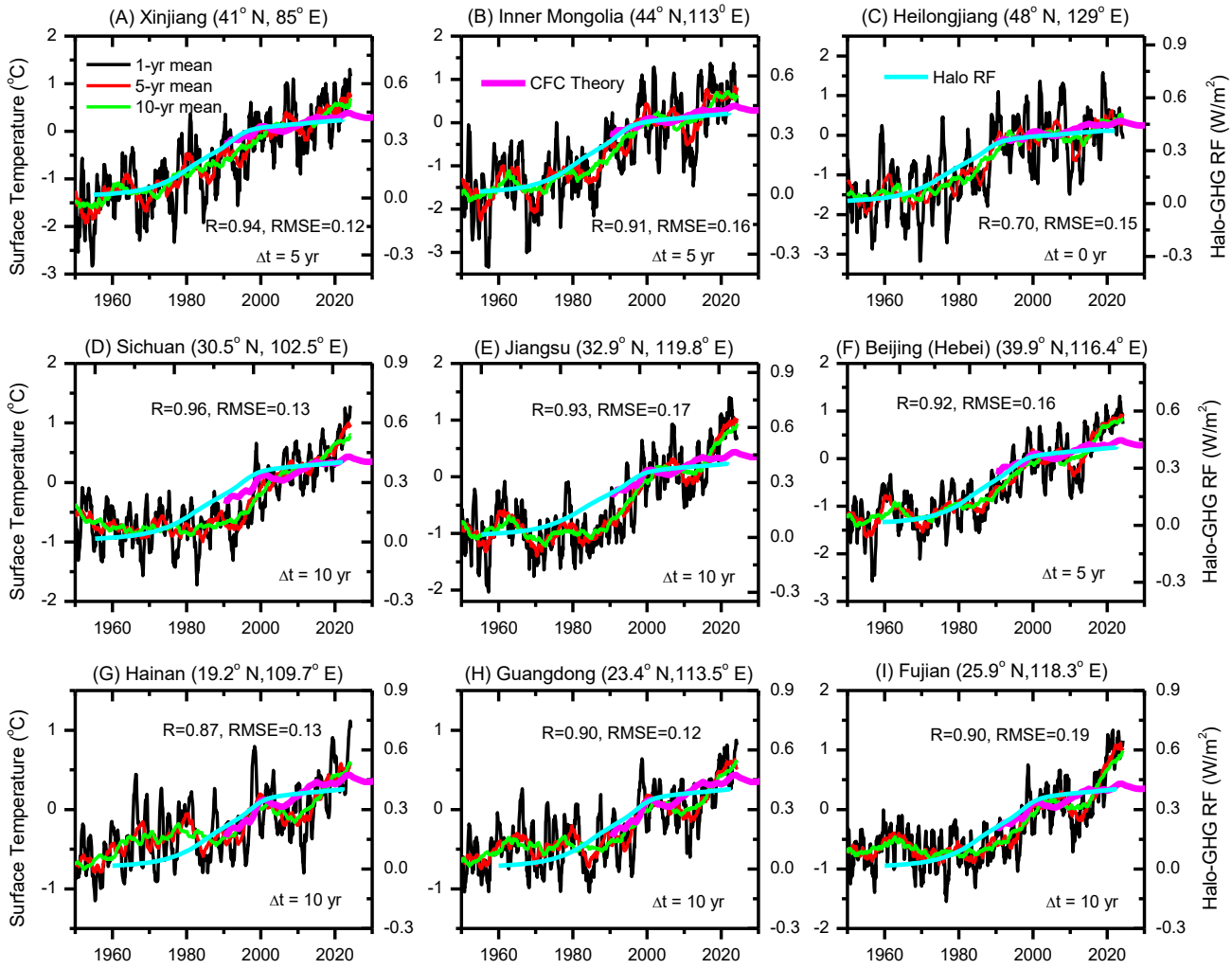

Figure 5. Time-series observed and calculated surface temperatures at the representative provinces/territories/cities of China, where the observed temperature data are processed by 1-, 5-, and 10-year smoothing, and time-series global mean (effective) radiative forcing (RF/ERF) of halo-GHGs is also shown with the lag (Δt) indicated. The temperatures are relative to their means in 1995–2005. In each of A-I, statistical analysis gives a linear correlation coefficient (R) and root mean square error (RMSE) for the observed 10-year mean GMSTs and no-parameter CFC model.

Finally, we note that warming in the surface temperature did not occur smoothly and slowly, but with abrupt ("step-wise") shifts (e.g., in 1998 and 2015/2016), which are more obvious over the tropics and northern midlatitudes. These abrupt changes are mainly caused by natural variability, including ENSO, the Pacific Decadal Oscillation (PDO), the Atlantic Multidecadal Oscillation (AMO), and the North Atlantic Oscillation (NAO) [4,32], showing that climate is a complex system, with a temporal evolution in which a small, even random, forcing could trigger rapid and irreversible changes (so-called "tipping points"). Moreover, persistent long-range power-law correlations of the temporal

fluctuations may also be hidden in the time-series residuals shown in Figure 6, which could be revealed by the DFA method [23]. Although these effects of internal variability (atmospheric dynamics) are not included in our theoretical calculations using Eq. 1, we believe that the trends in regional surface temperatures due to the anthropogenic halo-GHGs and aerosols are predictable in our CFC warming physics model and testable by future observed temperatures in this and coming decades.

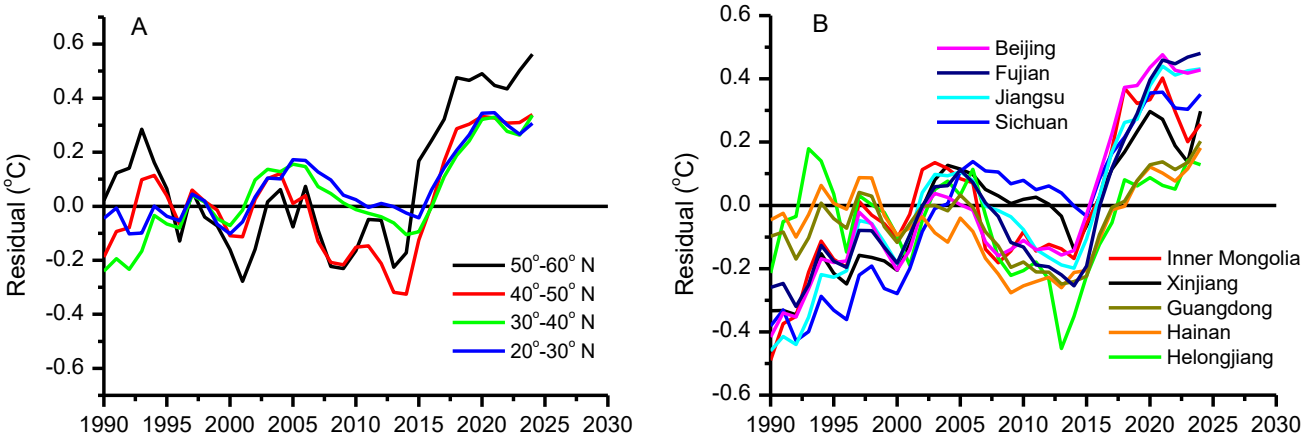

Figure 6. Residuals of observed surface temperatures after the subtraction of the CFC theoretical values.

4. Conclusions

In Summary, we present quantitative analysis of regional and provincial surface temperature changes in China. Our observations show that the surface temperature changes in China are highly inhomogeneous, exhibiting the major temporal patterns in regional climate change, which agree with the prediction by the CRE mechanism for decomposition of halo-GHGs in the stratosphere and troposphere. The complete quantitative CRE and CFC-warming theories [10,16,22] predicted that a reversal in climate change caused by halo-GHGs will be occurring earlier at regions of higher latitudes. However, this reversal is affected by recent drastic reductions in air pollution, which give rise to positive net radiative forcings. The latter are the primary cause for the recent rises in global mean surface temperature and in regional surface temperatures in China, as revealed in [12] and this study, respectively. Although only globally averaged effective radiative forcings of aerosols and ozone due to air pollution variations are used in this study, our theoretically calculated surface temperature changes since 1990 by the CFC-warming physics model have given results in overall good agreement with observations with given correlation coefficients at 0.70–0.96. In lightly polluted regions, such as northeast and northwest China, Hainan, and Guangdong, the calculated results closely reproduce the observed temperatures, whereas the calculated results underestimate the observed temperatures at highly polluted regions such as Beijing (Hebei) and eastern and southeast China (Fujian, Jiangsu, and Sichuan). This underestimate is reasonably explained by the much severer air pollution in these regions in China before 2013 than most rest parts of the globe, which gave rise to a larger positive net radiative forcing in the last decade. From these observed and calculated results, we conclude that not only global mean but also regional surface temperature changes have mainly been caused by anthropogenic halogenated gases, which are responsible for two major world-wide environmental problems: Ozone depletion and global

climate change. This study also highlights the valuable contribution of regional and global air quality monitoring (e.g., through the AERONET network [24]) and relevant studies on the impacts of emission changes on domestic and intercontinental air quality, climatic, and health effects [2,3] to the success of the Sustainable Development Goals-UN 2030 agenda. Further studies on the possible long-range power-law correlations of the temporal fluctuations in the detrended time-series GMST anomalies (e.g., by the DFA method [23]) could improve the accuracy of our model calculations to predict future climate changes.

Data Availability Statement

The data of aerosol optical depths (AOD) at measurement stations in China were obtained from the AERONET network (https://aeronet.gsfc.nasa.gov/data_menu.html); surface temperature data were obtained from Huang, B., X. Yin, M. J. Menne, R. Vose, and H. Zhang, NOAA Global Surface Temperature Dataset (NOAAGlobalTemp), Version 6.0.0 [Global Gridded 5° Monthly dataset], NOAA National Centers for Environmental Information, https://doi.org/10.25921/rzxg-p717; the data of TSI, concentrations of halogenated GHGs, effective radiative forcings of ozone and aerosols were obtained from the IPCC AR6 (https://www.ipcc.ch/report/ar6/wg1/) [4].

Author contributions

Q.L., K.D. and K.Z. designed research; K.Z. performed research; Q.L. contributed new reagents/analytic tools; K.Z. analyzed data; and K.Z. K.D. and Q.L. wrote the paper.

Use of AI tools declaration

The authors declare they have not used Artificial Intelligence (AI) tools in the creation of this article.

Acknowledgments

This research was funded by the Natural Science and Engineering Research Council of Canada and the University of Waterloo (QB Lu) and by the Project of Beijing Municipal Science & Technology Commission (#Z221100005222016) (KJ Ding).

Conflict of interest

The authors declare no conflicts of interest.

References

1. Ma X, Ortolano L (2000) *Environmental Regulation in China: Institutions, Enforcement, and Compliance*, New York: Rowman, 1–250. https://doi.org/10.1017/S0009443901220592

2. Zheng B, Tong D, Li M, et al. (2018) Trends in China's anthropogenic emissions since 2010 as the consequence of clean air actions. *Atmos Chem Phys* 18: 14095–14111. https://doi.org/10.5194/acp-18-14095-2018
3. Zhang Y, Shindell D, Seltzer K, et al. (2021) Impacts of emission changes in China from 2010 to 2017 on domestic and intercontinental air quality and health effect. *Atmos Chem Phys* 21: 16051–16065. https://doi.org/10.5194/acp-21-16051-2021
4. IPCC, Climate Change 2021—The Physical Science Basis: Working Group I Contribution to the Sixth Assessment Report of the Intergovernmental Panel on Climate Change, Cambridge: Cambridge University Press. 2023.
5. Lu QB (2023) Critical Review on Radiative Forcing and Climate Models for Global Climate Change since 1970. *Atmosphere* 14: 1232. https://doi.org/10.3390/atmos14081232
6. Yang Z, Zhang W, Villarini G (2023) Impact of coronavirus-driven reduction in aerosols on precipitation in the western United States. *Atmos Res* 288: 106732. https://doi.org/10.1016/j.atmosres.2023.106732
7. Wang P, Yang Y, Xue D, et al. (2023) Aerosols overtake greenhouse gases causing a warmer climate and more weather extremes toward carbon neutrality. *Nat Commun* 14: 7257. https://doi.org/10.1038/s41467-023-42891-2
8. Balaji V, Couvreux F, Deshayes J, et al. (2022) Are general circulation models obsolete? *Proc Natl Acad Sci* 119: e2202075119. https://doi.org/10.1073/pnas.2202075119
9. Lean JL, Rind DH (2008) How natural and anthropogenic influences alter global and regional surface temperatures: 1889 to 2006. *Geophys Res Lett* 35: L18701. https://doi.org/10.1029/2008GL034864
10. Lu QB (2015) *New Theories and Predictions on the Ozone Hole and Climate Change*, New Jersey: World Scientific, 1–285. https://doi.org/10.1142/9286
11. Lu QB (2022) Major Contribution of Halogenated Greenhouse Gases to Global Surface Temperature Change. *Atmosphere* 13: 1419. https://doi.org/10.3390/atmos13091419
12. Lu QB (2025) Contribution of shorter-term radiative forcings of aerosols and ozone to global warming in the last two decades. *AIP Adv* 15: 055224. https://doi.org/10.1063/5.0248842
13. Lu QB, Sanche L (2001) Effects of cosmic rays on atmospheric chlorofluorocarbon dissociation and ozone depletion. *Phys Rev Lett* 87: 078501. https://doi.org/10.1103/PhysRevLett.87.078501
14. Lu QB (2009) Correlation between Cosmic Rays and Ozone Depletion. *Phys Rev Lett* 102: 118501. https://doi.org/10.1103/PhysRevLett.102.118501
15. Lu QB (2021) Fingerprints of the cosmic ray driven mechanism of the ozone hole. *AIP Adv* 11: 115307. https://doi.org/10.1063/5.0047661
16. Lu QB (2023) Formulation of the cosmic ray–driven electron-induced reaction mechanism for quantitative understanding of global ozone depletion. *Proc Natl Acad Sci* 120: e2303048120. https://doi.org/10.1073/pnas.2303048120
17. Lu QB (2025) Cosmic ray–driven electron-induced reaction theory quantifies spatiotemporal variations in lower-stratospheric ozone and temperature. *Proc Natl Acad Sci* 122: e2506469122. https://doi.org/10.1073/pnas.2506469122
18. Banerjee A, Fyfe J, Polvani L, et al. (2020) A pause in Southern Hemisphere circulation trends due to the Montreal Protocol. *Nature* 579: 544–548. https://doi.org/10.1038/s41586-020-2120-4

19. Solomon S, Ivy D, Kinnison D, et al. (2016) Emergence of healing in the Antarctic ozone layer. *Science* 353: 269–274. https://doi.org/10.1126/science.aae0061
20. Philipona R, Mears C, Fujiwara M, et al. (2018) Radiosondes Show That After Decades of Cooling, the Lower Stratosphere Is Now Warming. *J Geophys Res Atmos* 123: 12509–12522. https://doi.org/10.1029/2018JD028901
21. Goessling HF, Rackow T, Jung T (2025) Recent global temperature surge intensified by record-low planetary albedo. *Science* 387: 68–73. https://doi.org/10.1126/science.adq7280
22. Lu QB (2026) *Theories and Predictions on Ozone Depletion and Climate Change*, New Jersey: World Scientific, 1–408. https://doi.org/10.1142/14613
23. Efstathiou MN, Tzanis C, Cracknell AP, et al. (2011) New features of land and sea surface temperature anomalies. *Int J Remote Sens* 32: 3231–3238. https://doi.org/10.1080/01431161.2010.541504
24. Giles DM, Sinyuk A, Sorokin MG, et al. (2019) Advancements in the Aerosol Robotic Network (AERONET) Version 3 database—automated near-real-time quality control algorithm with improved cloud screening for Sun photometer aerosol optical depth (AOD) measurements. *Atmos Meas Tech* 12: 169–209. https://doi.org/10.5194/amt-12-169-2019
25. Vose RS, Huang B, Yin X, et al. (2021) Implementing Full Spatial Coverage in NOAA's Global Temperature Analysis. *Geophys Res Lett* 48: e2020GL090873. https://doi.org/10.1029/2020GL090873
26. Huang B, Yin X, Menne MJ, et al. (2022) Improvements to the Land Surface Air Temperature Reconstruction in NOAAGlobalTemp: An Artificial Neural Network Approach. *Artif I Earth Syst* 1: e220032. https://doi.org/10.1175/AIES-D-22-0032.1
27. Yeh SW, Kug JS, Dewitte B, et al. (2009) El Niño in a changing climate. *Nature* 461: 511–514. https://doi.org/10.1038/nature08316
28. Rojo Hernández JD, Mesa ÓJ, Lall U (2020) ENSO Dynamics, Trends, and Prediction Using Machine Learning. *Wea Forecasting* 35: 2061–2081. https://doi.org/10.1175/WAF-D-20-0031.1
29. Douglass DH, Clader BD (2002) Climate sensitivity of the Earth to solar irradiance. *Geophys Res Lett* 29: 33-31–33-34. https://doi.org/10.1029/2002GL015345
30. Ball W, Alsing J, Mortlock D, et al. (2018) Evidence for a continuous decline in lower stratospheric ozone offsetting ozone layer recovery. *Atmos Chem Phys* 18: 1379–1394. https://doi.org/10.5194/acp-18-1379-2018
31. Ball W, Chiodo G, Abalos M, et al. (2020) Inconsistencies between chemistry-climate models and observed lower stratospheric ozone trends since 1998. *Atmos Chem Phys* 20: 9737–9752. https://doi.org/10.5194/acp-20-9737-2020
32. Varotsos CA, Franzke CLE, Efstathiou MN, et al. (2014) Evidence for two abrupt warming events of SST in the last century. *Theor Appl Climatol* 116: 51–60. https://doi.org/10.1007/s00704-013-0935-8